

Structure and mechanical properties of crab exoskeletons

Po-Yu Chen*, Albert Yu-Min Lin, Joanna McKittrick, Marc André Meyers

*Department of Mechanical and Aerospace Engineering and Materials Science and Engineering Program,
University of California, San Diego, La Jolla, CA 92093-0411, USA*

Received 15 June 2007; received in revised form 27 November 2007; accepted 18 December 2007
Available online 17 January 2008

Abstract

The structure and mechanical properties of the exoskeleton (cuticle) of the sheep crab (*Loxorhynchus grandis*) were investigated. The crab exoskeleton is a natural composite consisting of highly mineralized chitin–protein fibers arranged in a twisted plywood or Bouligand pattern. There is a high density of pore canal tubules in the direction normal to the surface. These tubules have a dual function: to transport ions and nutrition and to stitch the structure together. Tensile tests in the longitudinal and normal to the surface directions were carried out on wet and dry specimens. Samples tested in the longitudinal direction showed a convex shape and no evidence of permanent deformation prior to failure, whereas samples tested in the normal orientation exhibited a concave shape. The results show that the composite is anisotropic in mechanical properties. Microindentation was performed to measure the hardness through the thickness. It was found that the exocuticle (outer layer) is two times harder than the endocuticle (inner layer). Fracture surfaces after testing were observed using scanning electron microscopy; the fracture mechanism is discussed.

© 2008 Acta Materialia Inc. Published by Elsevier Ltd. All rights reserved.

Keywords: Arthropod exoskeletons; Biomineralization; Bouligand structure; Biological composite; Chitin

1. Introduction

Arthropods are the largest animal phylum. They include the trilobites, chelicerates, myriapods, hexapods, and crustaceans. All arthropods are covered by an exoskeleton, which is periodically shed as the animal grows. The exoskeleton of arthropods consists mainly of chitin. In the case of crustaceans, there is a high degree of mineralization, typically calcium carbonate, which gives mechanical rigidity.

The arthropod exoskeleton is multifunctional: it supports the body, resists mechanical loads, and provides environmental protection and resistance to desiccation [1–5]. The outermost region is the epicuticle, a thin, waxy layer which is the main waterproofing barrier. Beneath the epicuticle is the procuticle, the main structural part, which is primarily designed to resist mechanical loads. The procuticle

is further divided into two parts, the exocuticle (outer) and the endocuticle (inner), which have similar composition and structure. The endocuticle makes up around 90 vol.% of the exoskeleton. The exocuticle is stacked more densely than the endocuticle. The spacing between layers varies from species to species. Generally, the layer spacing in the endocuticle is about three times larger than that in the exocuticle [6]. Fig. 1a is a SEM micrograph showing the epicuticle, exocuticle, and endocuticle.

A striking feature of arthropod exoskeletons is their well-defined hierarchical organization, which reveals different structural levels, as shown in Fig. 1b. At the molecular level, there are long-chain polysaccharide chitins that form fibrils, 3 nm in diameter and 300 nm in length. The fibrils are wrapped with proteins and assemble into fibers of about 60 nm in diameter. These fibers further assemble into bundles. The bundles then arrange themselves parallel to each other and form horizontal planes. These planes are stacked in a helicoid fashion, creating a twisted plywood structure. A stack of layers that have completed a 180°

* Corresponding author. Tel.: +1 858 531 4571.
E-mail address: pochen@ucsd.edu (P.-Y. Chen).

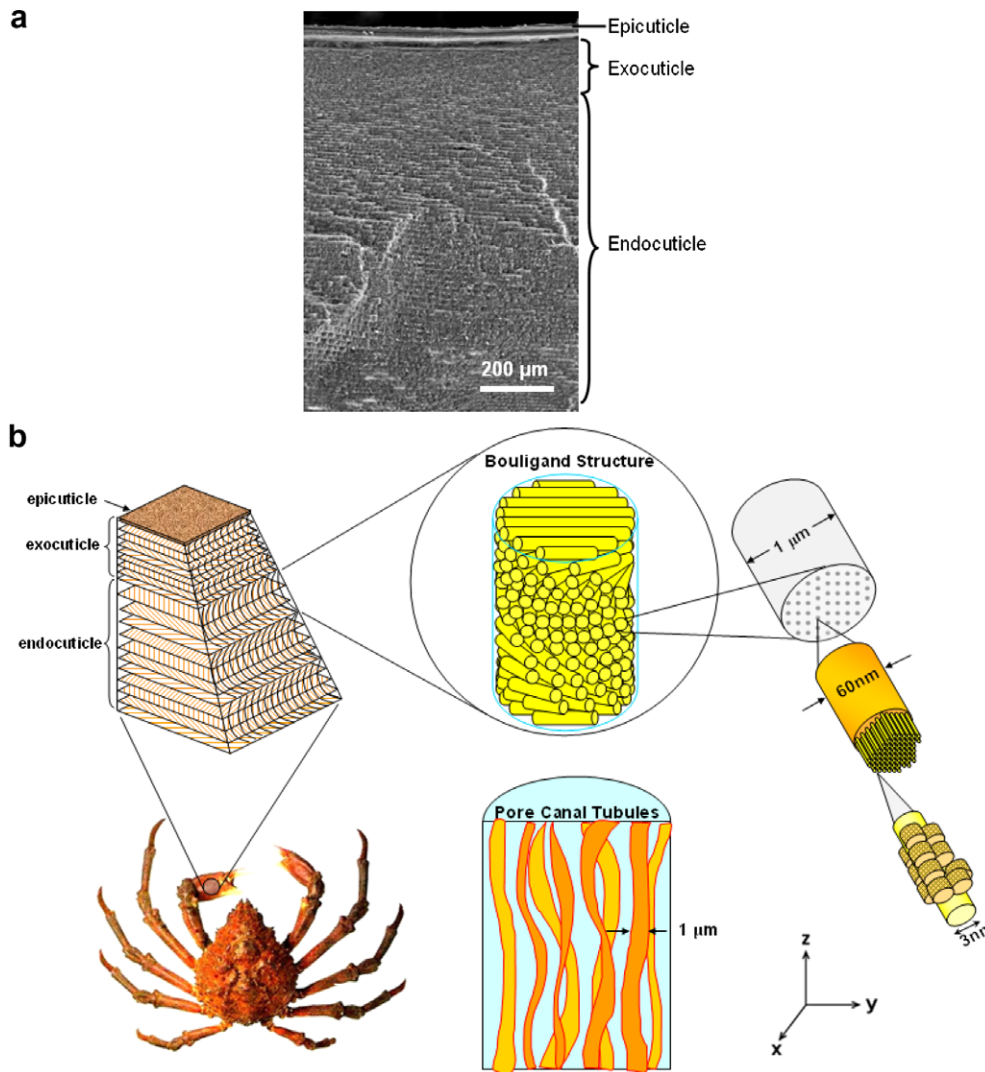


Fig. 1. (a) SEM micrograph of a cross-sectional fracture surface showing three different layers in the exoskeleton: epicuticle, exocuticle, and endocuticle. (b) Hierarchical structure of the exoskeleton of sheep crab, *Loxorhynchus grandis*. Chitin fibrils (~ 3 nm in diameter) wrapped with proteins form a fiber of ~ 60 nm in diameter. Fibers further assemble into bundles, which form horizontal planes (x - y plane) superposed in a helicoid stacking, creating a twisted plywood structure (180° rotation). In the z -direction there are ribbon-like tubules, $1 \mu\text{m}$ wide and $0.2 \mu\text{m}$ thick, running through the pore canals.

rotation is referred to as a Bouligand structure. These structures repeat to form the exocuticle and endocuticle [7–11]. The same Bouligand structure is also characteristic of collagen networks in compact bone, cellulose fibers in plant cell walls and other fibrous materials [12]. In crab exoskeletons, the minerals are in the form of calcite or amorphous calcium carbonate, deposited within the chitin–protein matrix [11,13–16].

In the direction normal to the surface (the z -direction), as shown in Fig. 1b, there are well-developed, high-density pore canals containing long, flexible tubules penetrating through the exoskeleton. These tubules play an important role in the transport of ions and nutrition during the formation of the new exoskeleton after the animals molt [17].

The mechanical properties of crustacean exoskeletons (mud crab, *Scylla serrata* and prawn, *Penaeus mondon*) were first investigated by Hepburn et al. [18] and Joffe

et al. [19]. Melnick et al. [20] studied the hardness and toughness of exoskeleton of the Florida stone crab, *Menippe mercenaria*, which exhibits a dark color (ranging from amber to black) on the chelae (tips of the claw) and walking legs. The dark material was much harder and tougher than the light-colored material from the same crab chela. The most comprehensive study is the one by Raabe and co-workers on the American lobster, *Homarus americanus* [6,21–25].

However, the mechanical properties in the direction normal to the surface have not yet been investigated. In this study, the mechanical properties of the sheep crab exoskeleton in the longitudinal direction (the y -direction) and the z -direction were measured. The exoskeleton is highly anisotropic, both in structure and mechanical properties. The motivation for this study is to understand the relationship between structure and mechanical properties in different

directions. The sheep crab (*Loxorhynchun grandis*), which resides in California and Baja California, was used for this study. The sheep crab can reach a maximum span of 1 m and a mass of about 4 kg [26,27]. The relatively large size and thick exoskeleton (the average thickness in the merus (top section) of the walking legs is about 2.5 mm) enable the mechanical tests in the z -direction. Another motivation for this investigation is the establishment of the mechanisms by which nature develops strong and tough materials using relatively weak (chitin, proteins and calcium carbonate) constituents. A range of hard natural materials has been investigated, such as the intricate tiled structure of the nacreous component of abalone shells [28–30], the sandwich structure of toucan beaks [31,32], silk [33] and others [2], yielding results that have significant technological applications.

2. Experimental methods

Three living adult male sheep crab, 15.4 ± 0.8 cm in carapace width, were obtained from a local seafood market. The crabs were in intermolt stage, in which the exoskeleton is completely developed and fully mineralized [11,34]. They were then kept in a 150 gallon tank with constant circulation of fresh sea water (mean temperature 16°C , mean salinity 33.60 ppt) and fed with fish weekly at the Scripps Institution of Oceanography until specimens were required. The tank was curtained, limiting the exposure to exterior lighting, creating a similar ambience to their natural habitat. Sample preparation was done as stated in the NIH Guide for Care and Use of Laboratory Animals.

The microstructure was characterized using a field emission scanning electron microscope (SEM) equipped with EDS (FEI-XL30, FEI Company, Oregon, USA). Samples were prepared as cross-sections and sections parallel to the surface. Both samples were cut from the ventral merus of the first walking leg. For the cross-sectional sample, a rectangular piece were obtained and then fractured in the longitudinal direction. For samples parallel to the surface, cylindrical pucks, 3 mm in diameter, were drilled using a diamond coring drill and fractured in tension. Samples were fractured immediately before examination with the SEM. The fractured samples were mounted on aluminum sample holders, air dried for 5 min and coated with 10 nm of gold in a sputter coater (Denton Discovery 18 Sputtering System, Denton Vacuum Inc., New Jersey, USA). Samples were observed with the secondary electron (SE) mode at 20 kV accelerating voltage.

Two sets of cross-sectional specimens (a total of six specimens from three different crabs) were prepared for microindentation. One was cut from the dorsal propodus (middle section) of the claw and the other was cut from the dorsal propodus of the second walking leg. The sample size was approximately $20\text{ mm} \times 5\text{ mm} \times 2\text{ mm}$ (length, width and thickness, respectively). Samples were mounted in epoxy with the cross-sectional area revealed, then ground and finely polished (Fig. 2a). A hardness testing

machine (LECO M-400-H1, Leco Co., Michigan, USA) equipped with a Vickers indenter was used. A load of 0.245 N was applied for 15 s, and a further 45 s was allowed to elapse before the diagonals of the indentation were measured. Twelve indentations were made through the thickness of exoskeleton at $100\ \mu\text{m}$ intervals and 10 parallel series of tests were performed on each sample (giving a total of 120 indentations). Two adjacent indentations were kept at least $100\ \mu\text{m}$ apart from each other to avoid the residual stress and strain hardening effect.

The specimens used for tensile and compressive testing in the longitudinal direction were taken from the merus of the first and second pairs of walking legs (Fig. 2). Tensile testing was carried out in the longitudinal direction of the crab walking legs, whereas tensile testing in the transverse direction was not conducted due to the limitation of sample size and curvature (the merus of walking legs is tubular in shape, about 12 cm in length and 2 cm in diameter). After muscle removal, the specimens were dissected into rectangles approximately 3 cm in length and 1 cm in width. The rectangles were ground to a thickness of about 1.8 mm and subsequently inserted into a laser cutting machine; the dog-bone shape, which was programmed into the machine, had a length of 25.4 mm, width of 6.35 mm, gage length of 6.35 mm and gage width of 2.29 mm. Thirty-four pieces were cut from three different crabs to prepare two equal sets of samples, one in a dry condition and one wet. Seventeen samples were air-dried, while others were kept in seawater to prevent desiccation during preparation. However, this could not be done for an indefinite period since the exoskeleton would become completely demineralized after several days. Therefore, for the hydrated condition, the testing was carried out within 24 h after the specimens were obtained.

The tensile tests in the longitudinal direction were performed on a specially designed fixture, consisting of two symmetric grips confined by a guiding track on the side. The grips were machined and had the same geometry as the dog-bone-shaped sample. The lower grip was fixed while the upper grip was movable and attached to a universal testing machine. The grips were designed in such a manner that the force was distributed evenly on the ends of specimens and this ensured that failure occurred in the reduced section. The grip design used also shielded specimens from bending, which could affect the results. A universal testing machine (Instron 3346 Single Column Testing Systems, Instron, MA, USA) equipped with a 500 N load cell was used. The crosshead speed was 0.03 mm/min, which corresponded to a strain rate of $7.9 \times 10^{-5}\ \text{s}^{-1}$.

Tensile testing was also carried out in the direction perpendicular to the surface (z -direction) as shown in Fig. 2c. Fifteen cylindrical pucks, 3.12 mm in diameter, were cut from the exoskeleton using a diamond coring drill. The epicuticle layer on the surface was removed leaving the exocuticle and endocuticle. The thickness of the samples is 2.50 ± 0.12 mm. These pucks were glued onto platens using

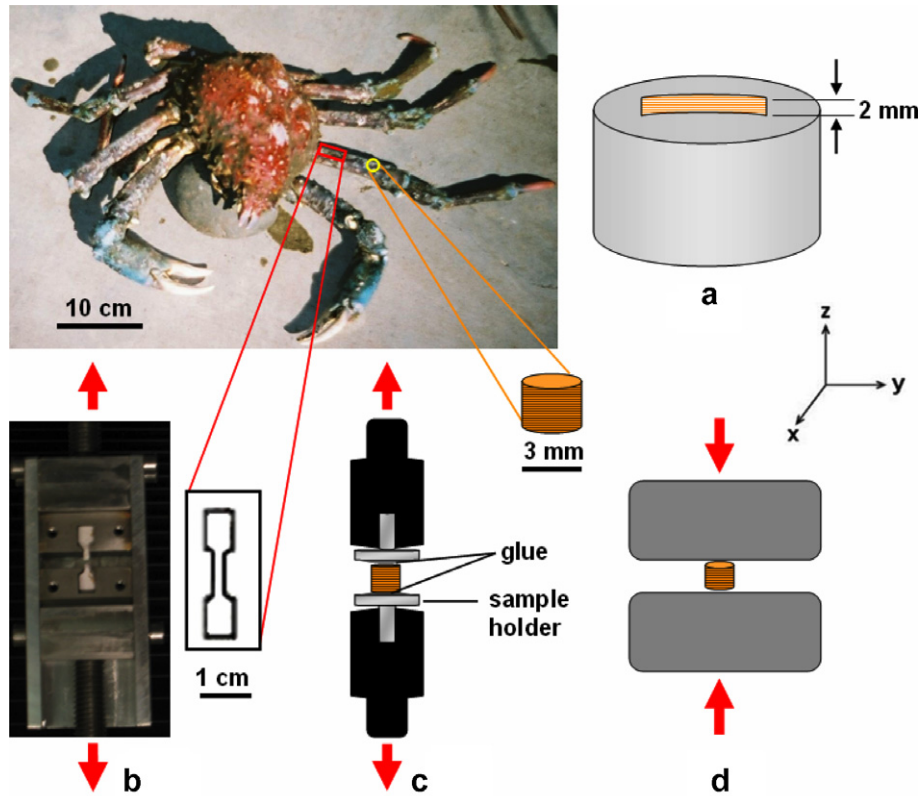


Fig. 2. Schematic representation of mechanical tests: (a) microindentation hardness test; (b) tensile test in the longitudinal direction; (c) tensile test in the z -direction; (d) compressive test in the z -direction.

Table 1
Mechanical properties of crab exoskeletons from tensile testing in the longitudinal direction

Sample	n	l (mm)	w (mm)	t (mm)	E (MPa)	σ_f (MPa)	ε_f (%)	Toughness (MPa)
Sheep crab wet	17	6.35 ± 0.01	2.29 ± 0.03	1.81 ± 0.09	518 ± 72	31.5 ± 5.4	6.4 ± 1.0	1.02 ± 0.25
Sheep crab dry	17	6.35 ± 0.01	2.29 ± 0.03	1.81 ± 0.10	764 ± 83	12.9 ± 1.7	1.8 ± 0.3	0.11 ± 0.03
Mud crab wet [17]					481 ± 75	30.1 ± 5.0	6.2	
Mud crab dry [17]					640 ± 89	23.0 ± 3.8	3.9	

The properties are the average including their standard deviation: l , gage length; w , gage width; t , thickness; E , Young's modulus. σ_f , stress to fracture; and ε_f , strain to fracture.

Table 2
Mechanical properties of crab exoskeletons from tensile testing in the z -direction

Sample	n	d (mm)	t (mm)	E (MPa)	σ_f (MPa)	ε_f (%)	Toughness (MPa)
Exo/endocuticle	15	3.12 ± 0.09	2.50 ± 0.12	511 ± 79	9.4 ± 2.6	2.0 ± 0.4	0.11 ± 0.04
Endocuticle	15	3.12 ± 0.08	2.48 ± 0.11	536 ± 87	19.8 ± 3.0	6.4 ± 1.6	0.78 ± 0.30

The properties are the average values including their standard deviation: d , diameter; t , thickness; E , Young's modulus. σ_f , stress to fracture; and ε_f , strain to fracture.

Table 3
Mechanical properties of crab exoskeletons from compressive testing in z -direction

Sample	n	d (mm)	t (mm)	E (MPa)	σ_y (MPa)	ε_y (%)	Toughness (MPa)
Sheep crab wet	17	3.11 ± 0.11	2.49 ± 0.09	634 ± 63	101 ± 11	15.7 ± 2.7	8.3 ± 1.5
Sheep crab dry	17	3.12 ± 0.10	2.49 ± 0.12	1069 ± 96	57 ± 10	5.2 ± 1.2	1.6 ± 0.5

The properties are the average values including their standard deviation: d , diameter; t , thickness; E , Young's modulus. σ_f , stress to fracture; and ε_f , strain to fracture.

J-B Weld® epoxy resin (J-B Weld Company, Texas, USA) and allowed to cure for 24 h. The platens were gripped to the universal testing machine and tested at a 0.03 mm/min crosshead speed. The fracture first occurred at the exocuticle–endocuticle interface. The exocuticle region was removed after fracture, leaving only the endocuticle region. Because the thickness of exocuticle is less than 200 μm , restricting the tensile testing, only the endocuticle region (2.48 ± 0.11 mm thick) was achievable. After the tensile tests, the fractured surfaces were sputter-coated with gold and characterized by SEM.

Compressive testing was conducted on the cylindrical samples in the z -direction (Fig. 2d). Two sets of samples, one in a dry condition and the other wet, were tested. A universal testing machine (Instron 3367 Dual Column Testing Systems, Instron, Massachusetts, USA) equipped with a 30 kN load cell was used. Specimens were tested at a 0.03 mm min^{-1} crosshead speed, which translated to a strain rate of $1.6 \times 10^{-4} \text{ s}^{-1}$. The dimensions of samples were summarized in Tables 1–3.

3. Results and discussion

3.1. Characterization of structure

Fig. 3a shows the lamellar structure in the endocuticle. Each layer corresponds to a 180° rotation of the twisted plywood (Bouligand) structure. A coordinate system is shown on the side. The spacing of layers in the exocuticle is approximately 3–5 μm , while that in the endocuticle is about 10–15 μm . Fig. 3b shows the Bouligand structure in detail. Fibers with diameter about 100 nm orient parallel to the x – y plane. These planes rotate gradually with respect to each other and form helical stacking. In the z -direction, there are pore canal tubules going through the layers. These pore canal tubules have a ribbon shape that twists in a helical fashion, as shown in Fig. 4a. The width of a single tubule is about 1 μm and the thickness is about 0.2 μm . A region where separation was introduced by tensile tractions is shown in Fig. 4b. These tubules are stretched and a necked configuration can be observed. The necking region is indicated by the arrows. Fig. 4c is the top view of the fracture surface (x – y plane) showing a high density of tubules. The area ratio of pore canals to chitin matrix is approximately 0.15, and the ratio of tubules to pore canals is approximately 0.50. It is estimated that there are about 1.5×10^{11} tubules per m^2 . The high density of tubules is also observed in other crabs. In the edible crab (*Cancer pagurus*), there are approximately 2×10^{11} tubules per m^2 [35]; in green crab (*Carcinus maenas*), there are about 9.5×10^{11} tubules per m^2 [36]. The tubules are the lighter segments protruding out of the pore canals. The neck cross-section is reduced to $0.01 \mu\text{m}^2$, a small fraction of the original area ($\sim 0.2 \mu\text{m}^2$). The necking of tubules is evidence of ductile failure; this ductile component plays a role in enhancing the toughness of the structure.

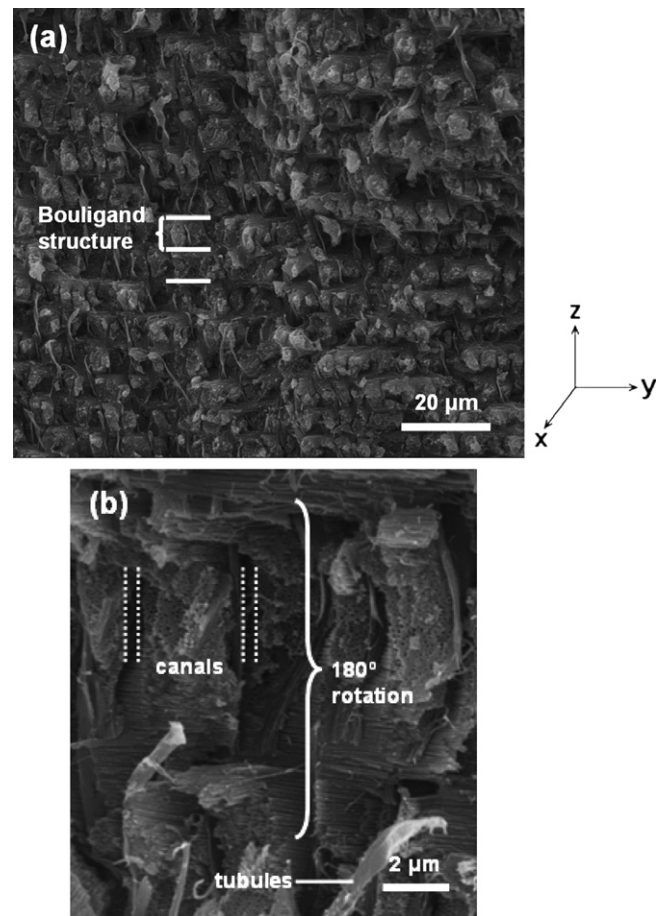


Fig. 3. (a) SEM micrograph showing the layered structure in endocuticle; (b) SEM micrograph showing the Bouligand structure, pore canals and pore canal tubules.

3.2. Mechanical testing

3.2.1. Microindentation

Fig. 5 shows the microindentation hardness through the thickness of the crab claws and walking legs. The data points are the average of 30 tests from three different samples and the scale bars are the standard deviations. The scanning electron micrograph of a cross-section is also shown in conjunction with the results. There is a discontinuity of hardness across the interface between the exocuticle and the endocuticle for both samples. The hardness values are 947 ± 74 MPa for claws and 247 ± 19 MPa for walking legs at 100 μm depths from the surface, which is in the exocuticle region (approximately 200 μm thick). They drop to a much lower value, 471 ± 50 MPa for claws and 142 ± 17 MPa for walking legs in the endocuticle (~ 2.5 mm thick). Thus, the hardness value in the exocuticle is about twice higher than that in the endocuticle. The discontinuity in hardness through the thickness of the crab exoskeleton is analogous to the results from American lobster (*H. americanus*) [6,23]. A qualitative energy-dispersive X-ray (EDX) mapping for calcium was carried out at the interface between the exocuticle and endocuticle of the

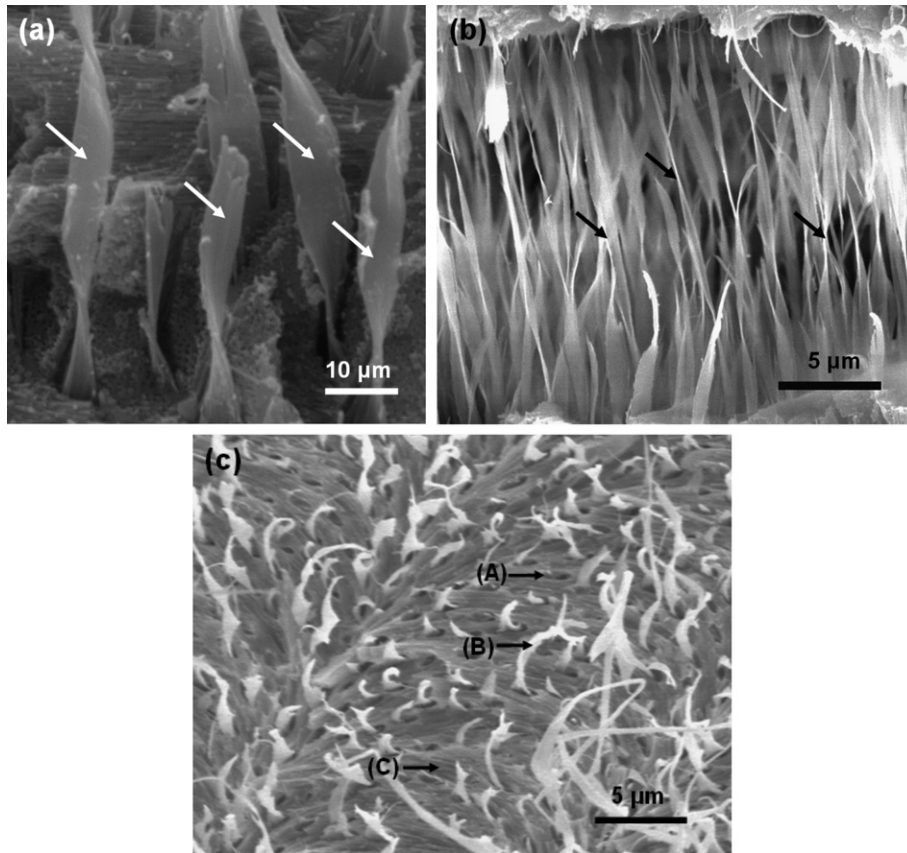


Fig. 4. SEM micrographs showing (a) ribbon-shaped pore canal tubules (arrows); (b) necked configuration of tubules in tensile traction (arrows); (c) top view of the pore canal tubules showing (A) pore canals; (B) pore canal tubules; (C) chitin fibers.

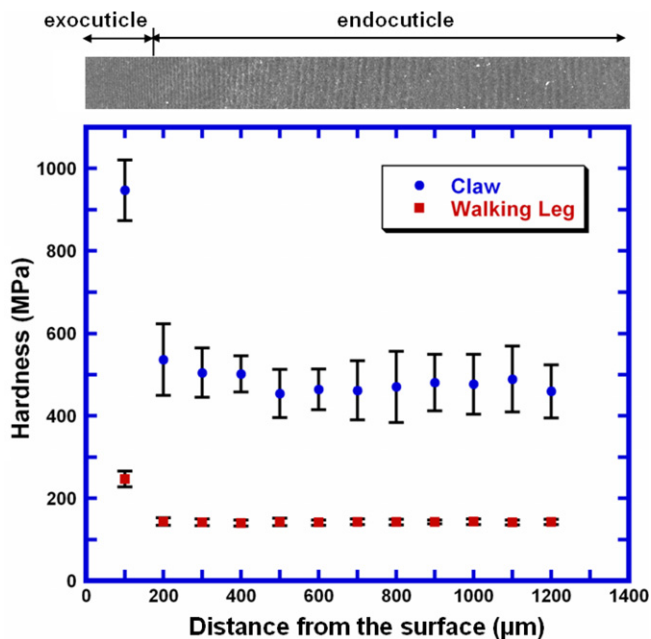


Fig. 5. Microindentation hardness showing a discontinuity through the thickness of crab claws and walking legs (data point: average; scale bar: standard deviation). The SEM micrograph above the plot documents the location where indentations were taken.

American lobster [23]. The result reveals a gradient in the calcium content between the exocuticle and endocuticle, indicating the exocuticle is more highly mineralized. Such design (higher hardness and wear resistance on the surface) is widely used in nature. For example, mammalian teeth are composed of external enamel and internal dentine. Enamel is hard and highly mineralized, while dentine is tougher and contains 30 vol.% of collagen. Another example is the smashing limb of the mantid shrimp, *Gonodactylus chiragra*, studied by Currey and co-workers [37]. The outer layer has a heavily calcified cuticle, with a significant amount of calcium carbonate being replaced by calcium phosphate. Beneath the outer layer is a fibrous region which absorbs the kinetic energy and prevents cracks from propagating through the cuticle. The smashing limb is well designed to break hard-shelled prey.

Another interesting discovery from the results is that the hardness values of the claw are about 3–4 times higher than those of the walking legs. The mineral content of the sheep crab exoskeleton was determined by heating a specimen at 400 °C for 8 h, and measuring the remaining ash weight. The average ash content of 15 pieces from the propodus of claws is $79.3 \pm 4.9\%$ of dry weight. The average ash content of 15 pieces from the merus of walking legs is $61.9 \pm 3.7\%$ of dry weight. The much higher hardness of the claw is likely due to the higher mineral content. The

hardness values measured in this work are higher than those of the American lobster claw (130–270 MPa in exocuticle and 30–55 MPa in endocuticle) [6]. This may also relate to the higher mineral content in sheep crab compared with the American lobster, which has an ash content of $63.6 \pm 4.3\%$ of dry weight [38].

3.2.2. Tensile testing

Typical stress–strain curves in the dry and wet conditions are shown in Fig. 6. They exhibit a slightly convex shape stress–strain response which corresponds to elastic deformation. Table 1 summarizes the mechanical properties of 34 tests taken from three different crabs. The wet samples have an average ultimate tensile strength of 31.5 ± 5.4 MPa at an average strain to fracture of $6.4 \pm 1.0\%$. The dry samples break at an average ultimate tensile strength of 12.9 ± 1.7 MPa at an average strain to fracture of $1.8 \pm 0.3\%$. The stress–strain curves for wet samples are not perfectly linear. This may be due to sample alignment at the initial stage. The Young's modulus was measured by taking the data points after 2% of strain and linear fitting. The average value of Young's modulus for the wet samples was 518 ± 72 MPa, whereas it was 764 ± 83 MPa for the dry samples. The work-of-fracture or toughness, as measured by the area under the stress–strain curve, is significantly affected by gradual fracture. The toughness for wet samples is 1.02 ± 0.25 MPa, which is almost 10 times higher than that for dry samples, which is 0.11 ± 0.03 MPa. Hepburn and co-workers [17] investigated the mechanical properties of mud crab, *S. serrata*, in tension. The stress–strain curves for both wet and dry mud crab samples are plotted in Fig. 6 along with the current results. There is a load drop in stress–strain curves at low strain. Hepburn et al. [17] concluded that this may be due to the failure of inorganic minerals at low strain, followed

by the fracture of chitin–protein matrix. However, the discontinuity is not observed in this study. The epicuticle and exocuticle were removed during the sample preparation and the stress–strain behavior reflected only the mechanical properties of the endocuticle. A discontinuity was observed in preliminary tests of whole crab exoskeletons. The exocuticle and the endocuticle fractured at low strain, while the epicuticle was still stretching and deforming.

The results of tensile testing in the *z*-direction are shown in Fig. 7 and mechanical properties are summarized in Table 2. For the cylindrical puck containing both exocuticle and endocuticle, the stress–strain curve is linear and fracture occurs at 9.4 ± 2.6 MPa and $2.0 \pm 0.4\%$ strain. For the sample that contains only endocuticle layers, the stress–strain curve shows a non-linear plastic deformation and the ultimate tensile strength reaches 19.8 ± 3.0 MPa and $6.4 \pm 1.6\%$ strain. The elastic modulus is 511 ± 79 MPa for exo/endocuticle samples and is 536 ± 87 MPa for endocuticle samples. Fracture tends to occur at the interface between the exocuticle and the endocuticle, where cracks can more easily propagate. The toughness of the sample containing both exocuticle and endocuticle is 0.11 ± 0.04 MPa. For the sample containing only endocuticle, the toughness is much higher, reaching 0.78 ± 0.30 MPa. It should be noted that both samples were tested in a dry condition since 24 h curing time is required.

3.2.3. Compression testing

Fig. 8 shows typical stress–strain curves in compression for both wet and dry crab exoskeletons in the *z*-direction. The results are summarized in Table 3. For wet samples, the average value of yield strength and Young's modulus are 101 ± 11 and 634 ± 63 MPa, respectively. For dry samples, average yield strength and Young's modulus are 57 ± 10 MPa and 1.07 ± 0.10 GPa, respectively.

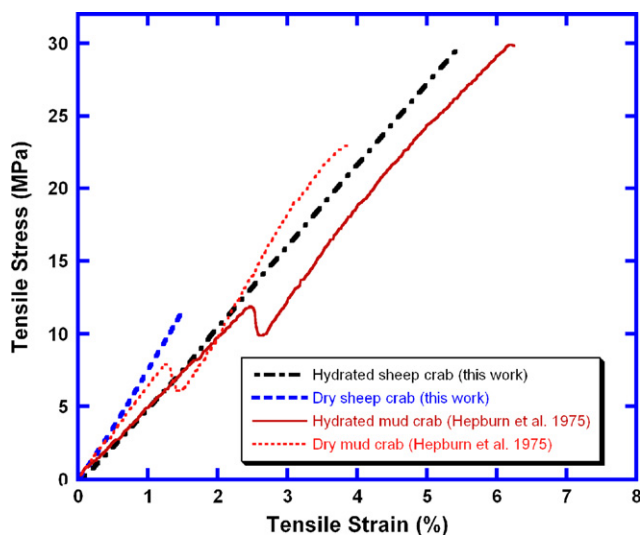


Fig. 6. Typical tensile stress–strain response of sheep crab exoskeleton in both dry and wet states in the *y*-direction. The results are compared with the mud crab exoskeleton by Hepburn et al. [18].

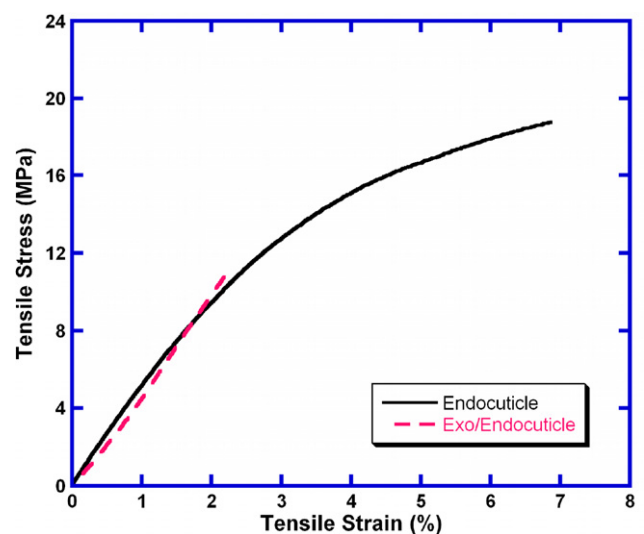


Fig. 7. Typical tensile response of sheep crab exoskeleton in the *z*-direction (dry condition).

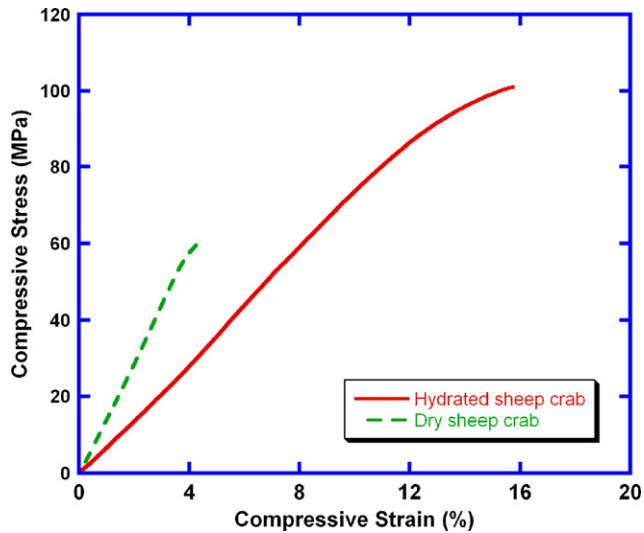


Fig. 8. Typical compressive stress–strain response of sheep crab exoskeleton in the z -direction (dry and wet conditions).

Compressive strength can be predicted from the Vickers hardness value, H_v , as $\sigma_c = H_v/3$. The average hardness of crab walking legs (in a dry condition) is 151 ± 30 MPa, corresponding to a predicted compressive strength of about 50 MPa, which is slightly lower than the measured value (57 ± 10 MPa). Both the strength and stiffness are higher in compression than in tension. The average toughness value of wet samples is 8.3 ± 1.5 MPa, whereas that of dry samples is 1.6 ± 0.5 MPa.

3.3. Fracture characterization and failure mechanisms

Fig. 9 shows the surface of a tensile specimen fractured in the longitudinal direction (dog-bone-shaped sample). The fracture surface of a dry sample is shown in Fig. 9a.

The typical twisted plywood structure can be observed. Chitin–protein bundles are broken apart, revealing a flat fracture surface. Fig. 9b shows the fracture surface of a wet sample, which is more irregular than the dry sample. Some chitin–protein bundles protruding out of the twisted plywood structure can be observed. The flat fracture surfaces shown in Fig. 9a and b are evidence of brittle fracture.

Fracture surfaces after tensile testing in the z -direction are shown in Fig. 10. Fig. 10a represents the fracture at the interface between the exocuticle and the endocuticle. There is a high density of pore canal tubules ruptured in tension and necking can be observed. The layered structure of the chitin–protein matrix in the exocuticle–endocuticle interface is smooth and flat. For the sample containing only endocuticle layers, the fracture surface of chitin–protein matrix is irregular and forms steps. A series of arced patterns can be observed in Fig. 10b. The arced pattern is produced by progressive rotation of layers and can be seen on the oblique surface of a Bouligand structure [7,9], as shown in Fig. 10c. Tubules fractured in ductile mode can also be observed in Fig. 10b. It is thought that tubules act as the ductile component that helps to stitch the brittle bundles together and provides the toughness in the z -direction.

Fig. 11 shows a schematic representation of the fracture processes. The breaking of chitin bundles when they are parallel to the loading direction (regions A in Fig. 9a) and their separation when they are parallel (regions B in Fig. 9a) are the main fracture modes. Intermediate orientations in the Bouligand will fail by either normal bundle fracture or bundle separation. Fracture in the x – y tensile specimens will preferentially travel through the orifices which provide the stress concentration sites. This is shown in Fig. 11a. For failure when loading is parallel to the z -direction (Fig. 11b), separation of the chitin bundles is fol-

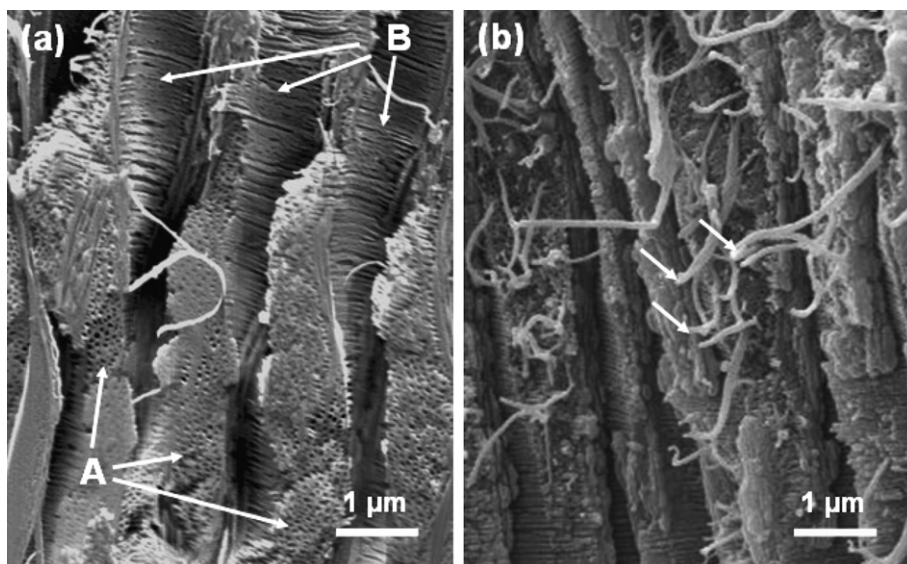


Fig. 9. Fracture surfaces of the exoskeleton in (a) dry and (b) wet conditions; A indicates chitin/mineral bundle fracture and B shows bundle separation.

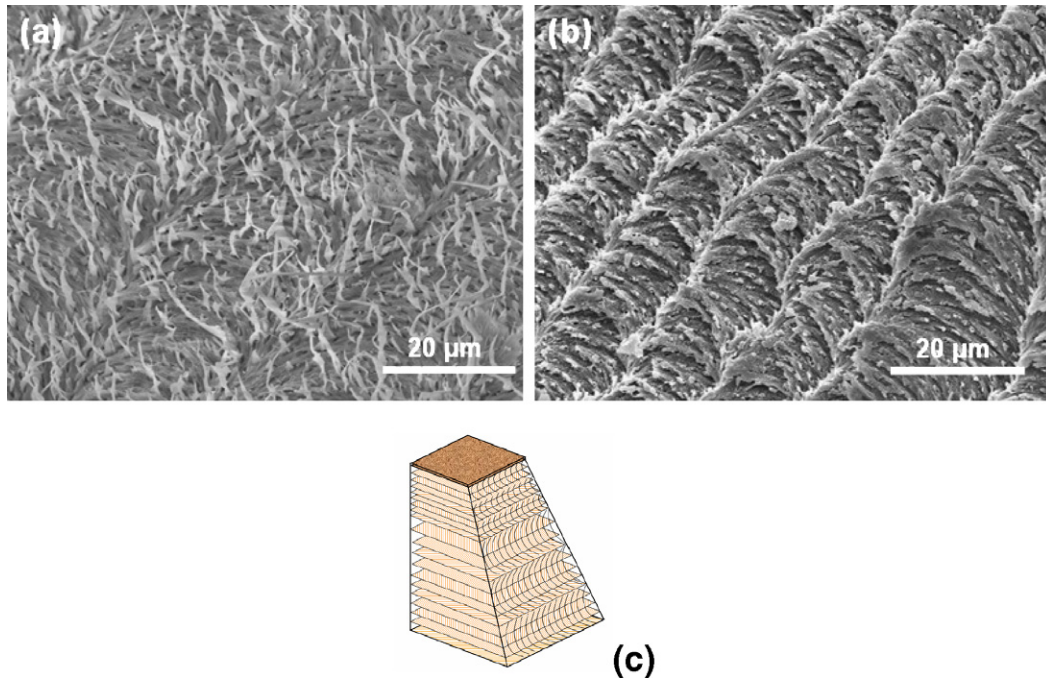


Fig. 10. Fracture surfaces of the exoskeleton after tensile test in the z -direction: (a) fracture between exocuticle and endocuticle; (b) fracture within endocuticle; (c) schematic drawing showing the arc pattern on oblique surface.

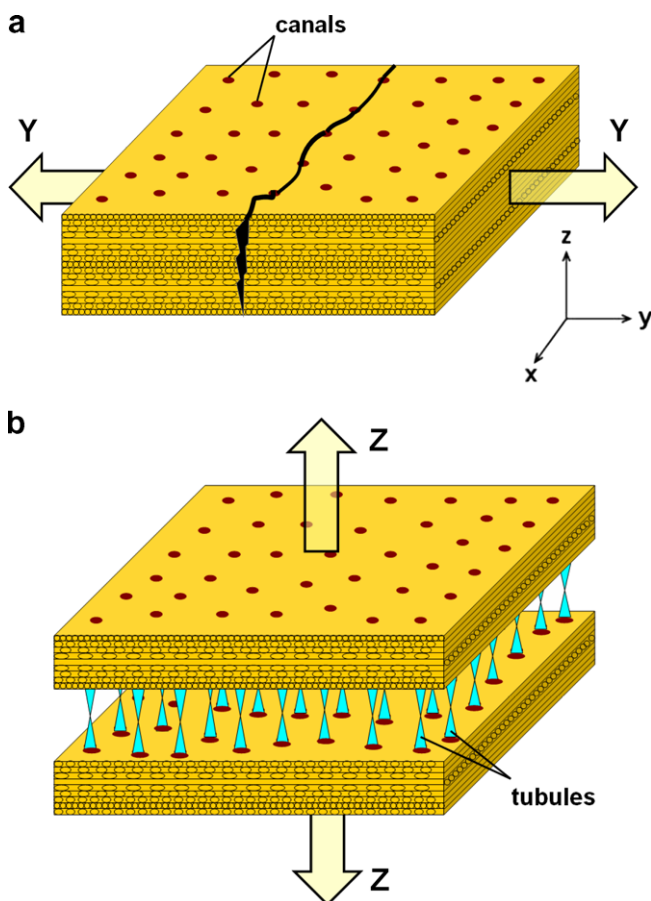


Fig. 11. Schematic drawings showing tensile failure in the (a) y -direction and (b) z -direction.

lowed by stretching of the tubules and their eventual failure. This provides an additional toughness to the network. The tensile strength of dry specimens in the x - y direction (12.9 MPa) is $\sim 50\%$ lower than that in the z -direction (19.8 MPa) because of unsupported brittle fracture of the chitin/mineral bundles, without the participation of the ductile tubules.

4. Conclusions

The principal conclusions are as follows:

- The crab exoskeleton is a three-dimensional composite comprising brittle chitin–protein bundles arranged in a Bouligand pattern (the x - y plane) and ductile pore canal tubules in the direction normal to the surface (the z -direction). The pore canal tubules possess ductile mechanical properties even in a dry condition.
- The Bouligand layers in exocuticle have a dense structure (3–5 μm each layer) and high hardness (947 MPa in claws and 247 MPa in walking legs). The endocuticle has a more open structure (10–15 μm each layer) and lower hardness (471 MPa in claws and 142 MPa in walking legs). The predicted compressive strength from hardness tests (50 MPa) is slightly lower than the measured values (57 MPa).
- The presence of water plays an important role in the mechanical properties. For both tensile and compressive tests, the wet samples have higher strength and toughness than the dry samples. The fracture surface of the dry samples is flat while for the wet samples it is irregular, due to some bundle pull-out.

- When tensile loading is applied in the *z*-direction, fracture tends to occur between the exocuticle and endocuticle interface and has a flat cleavage appearance. For the samples containing only endocuticle layers, the fracture morphology is irregular and there is non-linear (irreversible) plastic deformation shown in the stress–strain curve.
- The high density of pore canal tubules which fail in the ductile mode may play an important role in enhancing toughness in the *z*-direction.

The structure and mechanical properties of arthropod exoskeletons have been much studied; however, this is the first approach to studying the mechanical properties in different directions, especially in the *z*-direction, and correlating the mechanical properties with the well-defined structure at different hierarchical levels. It is important for materials scientists to understand the design of natural composites, in order to develop novel composite materials with enhanced properties.

Acknowledgements

We thank Evelyn York (Scripps Institution of Oceanography) and Ryan Anderson (CALIT2) for assistance with the scanning electron microscopy and Eddie Kisfaludy for maintaining the aquarium facility at the Scripps Institution of Oceanography. The authors gratefully acknowledge the support from the National Science Foundation Grant DMR 0510138. The valuable insights by the reviewers are gratefully acknowledged.

References

- [1] Neville AC. Biology of the arthropod cuticle. New York: Springer-Verlag; 1975.
- [2] Vincent JFV. Structural biomaterials. Princeton, NJ: Princeton University Press; 1991.
- [3] Vincent JFV. Arthropod cuticle: a natural composite shell system. *Composites A* 2002;33:1311–5.
- [4] Vincent JFV, Wegst UGK. Design and mechanical properties of insect cuticle. *Arthropod Struct Dev* 2004;33:187–99.
- [5] Sanchez C, Arribart H, Giraud-Guille MM. Biomimetic and bioinspiration as tools for the design of innovative materials and systems. *Nat Mat* 2005;4:277–88.
- [6] Raabe D, Sachs C, Romano P. The crustacean exoskeleton as an example of a structurally and mechanically graded biological nanocomposite material. *Acta Mater* 2005;53:4281–92.
- [7] Bouligand Y. Twisted fibrous arrangements in biological materials and cholesteric meso phases. *Tissue Cell* 1972;4:189–217.
- [8] Giraud-Guille MM. Fine structure of the chitin–protein system in the crab cuticle. *Tissue Cell* 1984;16:75–92.
- [9] Giraud-Guille MM. Chitin crystals in arthropod cuticles revealed by diffraction contrast transmission electron microscopy. *J Struct Biol* 1990;103:232–40.
- [10] Weiner S, Addadi L. Design strategies in mineralized biological materials. *J Mater Chem* 1997;7:689–702.
- [11] Roer R, Dillaman R. The structure and calcification of the crustacean cuticle. *Am Zool* 1984;24:893–909.
- [12] Giraud-Guille MM. Plywood structure in nature. *Curr Opin Solid State Mater Sci* 1998;3:221–8.
- [13] Lowenstam HA. Minerals formed in organisms. *Science* 1981;211:1126–31.
- [14] Mann S, Webb J, Williams RJP. On biomineralization. New York: VCH; 1989.
- [15] Lowenstam HA, Weiner S. On biomineralization. New York: Oxford University Press; 1989.
- [16] Giraud-Guille MM, Bouligand Y. Crystal growth in a chitin matrix: the study of calcite development in the crab cuticle. In: Karnicki ZS, Brzeski PJ, Wojtasz-Pajak A, editors. *Chitin World*. Bremerhaven: Wirtschaftsverlag NW; 1994. p 136–144.
- [17] Cameron JN. Post-molt calcification in the blue crab, *Callinectes sapidus* – timing and mechanism. *J Exp Biol* 1989;143:285–304.
- [18] Hepburn HR, Joffe I, Green N, Nelson KJ. Mechanical properties of a crab shell. *Comp Biochem Physiol* 1975;50A:551–4.
- [19] Joffe I, Hepburn HR, Nelson KJ, Green N. Mechanical properties of a crustacean exoskeleton. *Comp Biochem Physiol* 1975;50A:545–9.
- [20] Melnick CA, Chen S, Mecholsky JJ. Hardness and toughness of exoskeleton material in the stone crab *Menippe mercenaria*. *J Mater Res* 1996;11:2903–7.
- [21] Raabe D et al. Discovery of a honeycomb structure in the twisted plywood patterns of fibrous biological nanocomposite tissue. *J Cryst Growth* 2005;283:1–7.
- [22] Raabe D et al. Structure and crystallographic texture of arthropod bio-composites. *Mater Sci Forum* 2005;495–497:1665–74.
- [23] Raabe D et al. Microstructure and crystallographic texture of the chitin–protein network in the biological composite material of the exoskeleton of the lobster *Homarus americanus*. *Mater Sci Eng A* 2006;421:143–53.
- [24] Sachs C, Fabritius H, Raabe D. Hardness and elastic properties of dehydrated cuticle from the lobster *Homarus americanus* obtained by nanoindentation. *J Mater Res* 2006;21:1987–95.
- [25] Romano P, Fabritius H, Raabe D. The exoskeleton of the lobster *Homarus americanus* as an example of a smart anisotropic biological material. *Acta Biomater* 2007;3:301–9.
- [26] Jensen GC. Pacific Coast Crabs and Shrimps. Monterey: Sea Challengers; 1995.
- [27] Debelius H. Crustacea: Guide of the World. Frankfurt: IKAN–Unterwasserarchiv; 2001.
- [28] Menig R, Meyers MH, Meyers MA, Vecchio KS. Quasi-static and dynamic mechanical response of *Haliotis rufescens* (abalone) shells. *Acta Mater* 2000;45:2389–98.
- [29] Mayer G. Rigid biological systems as models for synthetic composites. *Science* 2005;310:1144–7.
- [30] Mayer G. New classes of tough composite materials – lessons from nature rigid biological systems. *Mater Eng Sci C* 2006;26:1261–8.
- [31] Seki Y, Schneider MS, Meyers MA. Structure and mechanical properties of the toucan beak. *Acta Mater* 2005;53:5281–96.
- [32] Seki Y, Kad B, Benson D, Meyers MA. The toucan beak: structure and mechanical response. *Mater Sci Eng C* 2006;26:1412–20.
- [33] Altman GH et al. Silk-based biomaterials. *Biomaterials* 2003;24:401–16.
- [34] Drach P. Mue et cycle d’intermue chez les crustacé decapods. *Ann Inst Oceanogr* 1939;19:103–391.
- [35] Hegdahl T, Silness J, Gustavsen F. The structure and mineralization of the carapace of the crab (*Cancer pagurus* L) – 1. The endocuticle. *Zool Scr* 1977;6:89–99.
- [36] Roer RD. Mechanisms of resorption and deposition of calcium in the carapace of the crab *Carcinus maenas*. *J Exp Biol* 1980;88:205–18.
- [37] Currey JD, Nash A, Bonfield W. Calcified cuticle in the stomatopod smashing limb. *J Mater Sci* 1982;17:1939–44.
- [38] Hayes DK, Armstrong WD. The distribution of mineral material in the calcified carapace and claw shell of the American lobster, *Homarus americanus*, evaluated by means of microx-ray fluorescence. *Bio Bull* 1961;121:307–15.